Quaternary Science Reviews 279 (2022) 107383

Contents lists available at ScienceDirect

Quaternary Science Reviews

journal homepage: www.elsevier.com/locate/quascirev

Paleoclimatic and paleoenvironmental changes in Amazonian lowlands over the last three millennia

Marcela Eduarda Della Libera [a, b, *], Valdir Felipe Novello [c], Francisco William Cruz [a], Rebecca Orrison [d], Mathias Vuille [d], Shira Yoshi Maezumi [e], Jonas de Souza [f], Julio Cauhy [b], José Leandro Pereira Silveira Campos [a], Angela Ampuero [a], Giselle Utida [a], Nicolás Misailidis Stríkis [g], Cintia Fernandes Stumpf [h], Vitor Azevedo [i], Haiwei Zhang [j], R. Lawrence Edwards [k], Hai Cheng [j, k]

[a] Institute of Geosciences, University of São Paulo, São Paulo, 05508-080, Brazil
[b] Institute for Geosciences, Johannes-Gutenberg Universtiät, Johann-Joachim-Becher-Weg 21, 55128, Mainz, Germany
[c] Department of Geosciences, University of Tübingen, Tübingen, 72076, Germany
[d] Department of Atmospheric and Environmental Sciences, University at Albany, Albany, NY, 12222, USA
[e] Department of Ecosystem and Landscape Dynamics, University of Amsterdam, 1090 GE, Amsterdam, the Netherlands
[f] Department of Humanities, Universitat Pompeu Fabra, Barcelona, 08002, Spain
[g] Departamento de Geoquímica, Universidade Federal Fluminense, Niterói, 24020-150, Brazil
[h] Instituto de Geociências, Universidade de Brasília, Brasília, 70297-400, Brazil
[i] Department of Geology, Trinity College Dublin, Dublin, D02 PN40, Ireland
[j] Institute of Global Environmental Change, Xi'an Jiaotong University, Xi'an, 710049, China
[k] Department of Earth Sciences, University of Minnesota, Minneapolis, MN, 55455, USA

ARTICLE INFO

Article history:
Received 24 November 2021
Received in revised form
14 January 2022
Accepted 15 January 2022
Available online 29 January 2022

Handling Editor: Mira Matthews

Keywords:
Holocene
Paleoclimatology
South America
Speleothems
Stable isotopes
Paleoenvironment
South American Monsoon system
Amazon
Archaeology
Vegetation dynamics

ABSTRACT

The paleoclimatic and paleoenvironmental history of the Amazon basin over the last millennia and the behavior of the South American Monsoon System (SAMS) throughout the lowlands have not yet been thoroughly examined due to a lack of records from more central portions of the basin. Here we discuss these past changes based on new high-resolution $\delta^{18}O$ and $\delta^{13}C$ records from speleothems collected in the southwestern Amazon Basin, at the core region of the convective activity of the SAMS. We demonstrate that the $\delta^{18}O$ from these new records is representative of SAMS variations and that this convective system provides distinct precipitation patterns over the basin. The SAMS was in a neutral phase with homogeneous precipitation between 1000 BCE and 300 CE, whereas drier conditions prevailed over the western side of the basin between 700 and 1200 CE and an east-west climatic dipole was established over the Amazon Basin after 1450 CE when wetter conditions prevailed over our study site. The speleothem $\delta^{13}C$ record indicates an overall tendency toward a more humid tropical forest during the studied period, except for a drier period which correlates with the Medieval Climate Anomaly (MCA). The dynamics of pre-Columbian cultures from southwestern Amazonia seem to have been related to paleoclimatic and environmental changes reported for the region.

1. Introduction

The Amazon Basin holds the world's largest tropical forest and due to its broad extension and equatorial location, the forest is a major center of deep atmospheric convection, playing an important role in global climate regulation and atmospheric dynamics (Werth and Avissar, 2002). The Amazonian region accounts for much of the hydroclimate variability and rainfall balance over South America, with several of its large demographic centers relying on its moisture supply (Salati et al., 1979; Carvalho et al., 2002; Liebmann et al.,

* Corresponding author. Institute of Geosciences, University of São Paulo, São Paulo, 05508-080, Brazil.
E-mail address: marcela.eduarda.godoy@usp.br (M.E. Della Libera).

https://doi.org/10.1016/j.quascirev.2022.107383
0277-3791/

2004; Marengo et al., 2012; Carvalho and Dias, 2020). Therefore, the thorough investigation of past climate over the basin, both on centennial and millennial timescales, is essential in order to understand its spatiotemporal variability, and how past climate and environmental changes affected pre-Columbian populations, their cultures, migrations and land-use systems (Maezumi et al., 2018; de Souza et al., 2019; Iriarte et al., 2020). In addition, this long-term historical perspective allows putting projected future social, economic, and environmental impacts of climate change throughout South America in a long-term context (Iriarte et al., 2020).

Records of past climate change on orbital (Cheng et al., 2013a; Cruz et al., 2009) and millennial timescales (Novello et al., 2018) show evidence of distinct rainfall variations over the continent related to changes in the South American Monsoon System (SAMS), which is the main climatic feature over the continent during austral summer-early autumn (JFM). These changes were likely related to changes in tropical Atlantic sea surface temperatures and regional atmospheric circulation (Cruz et al., 2009; Bird et al., 2011; Marengo et al., 2012; Vuille et al., 2012; Novello et al., 2012, 2018; Kanner et al., 2013; Zilli et al., 2019). Studies based on high-resolution stalagmite $\delta^{18}O$ records have investigated changes in SAMS activity, both over the last two millennia (e.g. Vuille et al., 2012; Thompson et al., 2013; Novello et al., 2012, 2016, 2018; Campos et al., 2019, Fig. 1) and on longer millennial-to orbital time scales (e.g. Cruz et al., 2009; Cheng et al., 2013b). These studies have identified a pervasive east-west precipitation dipole over South America due to changes in SAMS activity characterized by increased rainfall over the western Amazon and a deficit recorded in Northeastern Brazil (NEB) and the eastern Amazon, and vice-versa. Moreover, Novello et al. (2018) explored the southwest-northeast shifts of the South Atlantic Convergence Zone (SACZ) during the past two millennia as evidence for changes in SAMS intensity, since the SACZ is a major monsoonal feature. Enhanced SAMS activity occurs in tandem with a southwestward displacement of the SACZ, thus reinforcing the precipitation dipole (Novello et al., 2018; Campos et al., 2019).

The paleoclimate studies covering the last millennia mentioned above, although of great relevance for the understanding of the SAMS, are either located far to the west in the Peruvian Andes (e.g.: Bird et al., 2011; Kanner et al., 2013; Thompson et al., 2013), or far to the east in NEB (e.g. Novello et al., 2012), or in central-western Brazil (e.g. Novello et al., 2016), leaving an informational gap in the more central locations in the Amazon lowlands. Therefore, the past SAMS behavior over lowland Amazonia, which is located at the node of the South American climate dipole, is not well represented in the current paleoclimate archives. The only cave study that addresses paleoclimatic changes within the Amazon basin lowlands is based on a high-resolution paleoclimatic record from Paraíso cave (Wang et al., 2017), which is**,** nevertheless, situated in the northeastern Amazon basin (within the eastern domain of the climate dipole). Additionally, Wang et al. (2017) do not discuss late-Holocene climatic changes in depth, and relate the $\delta^{18}O$ differences between sites located in the eastern and western Amazon over millennial time-scales to the impact of long-term vegetation changes on the isotopic gradient across the basin, thus providing a different interpretation from other $\delta^{18}O$ isotopic records covering the last millennia. Therefore, given the scarcity of records in the central/southwestern Amazon lowlands and the diverging previous interpretations, further investigation based on new high-resolution records in this area is needed to better understand the spatial variability of Amazonian paleoclimatic changes.

In addition to changes in SAMS activity over the southwestern Amazon lowlands, this region is characterized by a vegetation ecotone zone between the Amazon rainforest and the Cerrado biome, the two main biomes of the continent. Changes between these two biomes have been approached by previous studies (Mayle et al., 2000; Burbridge et al., 2004), yet over millennial timescales. Discussions regarding centennial-scale changes in vegetation for the late-Holocene (last 3 millennia) have focused only on low-resolution pollen records, which indicate a progressive southward expansion of the Amazonian rainforest for this period (Mayle et al., 2000; Burbridge et al., 2004; Carson et al., 2014). A high-resolution record to better assess the vegetation response to changes in climate, particularly in the SAMS domain, is thus lacking.

Important questions remain regarding the climatic and environmental conditions over the Amazon Basin during the past millennia, such as: 1) What paleoclimatic conditions prevailed in the Amazon lowlands near the node of the South American precipitation dipole? 2) Did changes in forest density affect the Amazonian $\delta^{18}O$ records during the last millennia, as suggested for millennial time-scales? 3) How did local hydroclimate, SAMS, vegetation and human activity interact in this region?

This study presents a new high-resolution speleothem record from a lowland region located in southwestern Brazilian Amazonia spanning the last 3 millennia**.** We further employ an isotope-enabled climate model to analyze the history of environmental and climatic changes in this region over the last millennium (Fig. 1). Our data is based on $\delta^{18}O$ and $\delta^{13}C$ analyses from stalagmites collected in a cave at the core of the SAMS domain, filling an important gap along an east-west paleoclimatic transect between the Amazon and surrounding regions. .

2. Samples, study site and modern climatology

The current study is based on two stalagmites (PIM4 and PIM5; Fig. S1) collected in Cuíca cave (11°40′S, 60°38′W, ~310 m a.s.l.) located in Pimenta Bueno city, Rondônia State, SW Amazon region in Brazil (Fig. 1). The stalagmites were collected in a chamber located ~200 m from the cave entrance, accessed by a narrow conduct upstream of the underground river that is episodically subject to flooding. Both samples are formed without major growth axis shifts, apparently as a result of a single dripping point each; both present a general light-orange opaque color tone, with growth layers evident in both speleothems. PIM4 is a 12.5 cm tall, conical-shaped stalagmite, which was still active by the time it was collected, with growth layers presenting a consistent conical geometry with no evidence of dissolution, yet with difference in coloration of the growth layers, being the bottom-half predominantly translucent/light orange, and the upper-half a opaque/darker orange. PIM5 is a 34 cm tall, conical-shaped stalagmite not active at time of collection, with growth layers displayed in a general flat-conical shape, with two visible detritus layers at the beginning of the sample. The cave site is located within the southwestern border of the Amazon Rainforest ecotone near the Cerrado (Brazilian savanna) biome. The vegetation is transitional, merging two of the most important Brazilian vegetation classifications; the Amazonian ombrophilous forest and the Central Plateau Cerrado (Miranda, 2000). Located within the core SAMS region, the rainy season, as recorded at nearby Pimenta Bueno city (11°40′S, 61°11′W, located at 60 km distance from the cave site) is therefore mainly controlled by the monsoon regime (Vera et al., 2006; Raia and Cavalcanti, 2008), and the climate is characterized as tropical humid with an annual average temperature of 26 °C. The average annual rainfall amount is about 1800 mm, 90% of which falls between October and April during the summer monsoon season (Fig. S2).

The core SAMS region is defined by the unique shift in low-level (850 hPa) wind direction that occurs in the southwestern Amazon from easterlies (JJA) to westerlies (northwesterlies over the continent) during the monsoon period (Raia and Cavalcanti, 2008). The

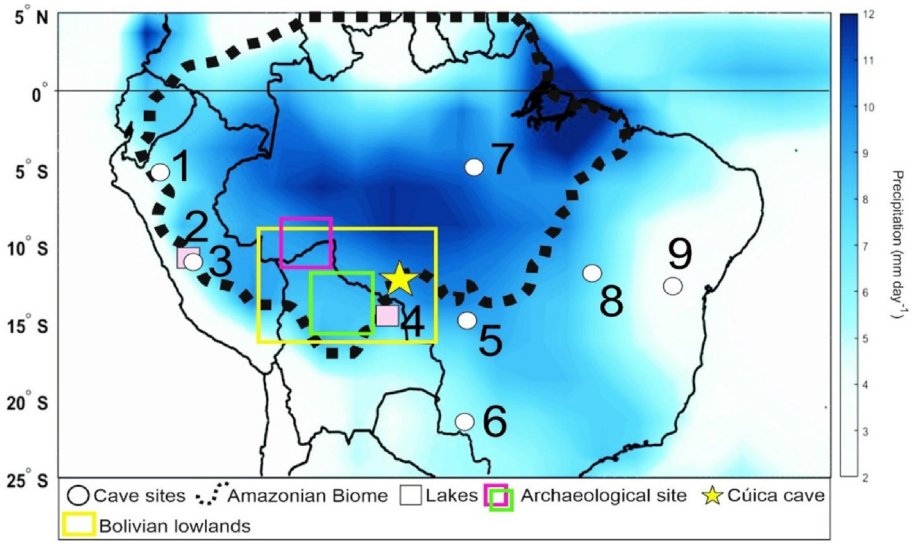

Fig. 1. Map of the tropical portion of South America with the locations of the records used in this study and the precipitation distribution in mm/day based on GPCP data during austral summer (JFM), when the SAMS is most active over the continent. The yellow star indicates the location of our speleothem site in Rondônia state. The other sites are 1) Palestina cave (Apaéstegui et al., 2014); 2) Pumacocha lake (Bird et al., 2011); 3) Huagapo cave (Kanner et al., 2013); 4) Laguna Chaplin (Maezumi et al., 2018); 5) Pau d'Alho and Curupira caves (Novello et al., 2016); 6) Jaraguá cave (Novello et al., 2018); 7) Paraíso cave (Wang et al., 2017); 8) Mata Virgem cave (Azevedo et al., 2019); 9) Diva de Maura cave (Novello et al., 2012). The yellow square indicates the archeological region in the Bolivian lowlands discussed in Maezumi et al. (2018); the pink square denotes the southwestern Amazon and the green square shows the Llanos de Moxos archeological regions. The black dashed line represents the Amazonian biome's current limits. (For interpretation of the references to color in this figure legend, the reader is referred to the Web version of this article.)

maximum influx of moisture from the tropical Atlantic occurs along the northern coast of South America and a more northerly trade wind component transports moisture southwestward into Amazonia, where strong convective activity takes place (Gan et al., 2004; Vera et al., 2006; Marengo et al., 2012; Vuille et al., 2012; Carvalho and Dias, 2020). The low-level convergence over the monsoon exit region produces the SACZ, a key monsoonal feature characterized by persistent convection and an elongated zone of precipitation extending from the monsoon region southeastward across the continent into the subtropical Atlantic Ocean, providing significant amounts of moisture to central and southeastern Brazil (Liebmann et al., 2004; Gan et al., 2004; Marengo et al., 2012; Carvalho and Dias, 2020).

3. Methods

3.1. Geochronology and composite

The geochronology of both PIM4 and PIM5 was established by means of the U/Th dating method, using an inductively coupled plasma-mass spectrometry (ICP-MS) technique at the Geochronology Laboratory at the University of Minnesota (USA) and at the Institute of Global Environmental Change, Xi'an Jiaotong University (China), following the methodology of Cheng et al. (2013a). The sampling for the U/Th dating was performed by extracting ~100 mg of powdered carbonate with a dentist drill along each stalagmite growth axis (21 U/Th ages for PIM4 and 16 for PIM5; Fig. S3), aiming to limit each sampling to a single growth layer or intercepting as few layers as possible. The $\delta^{18}O$ and $\delta^{13}C$ analyses were performed at the Stable Isotope Laboratory at the Institute of Geoscience of the University of São Paulo (Brazil) using a Thermo-Finnigan Delta Plus Advantage mass spectrometer. The notation δ in the results refers to the relative Vienna Pee Dee Belemnite (VPDB) standard with the per mil deviation, with uncertainties on the values of 0.1‰ for both analyses. 706 samples of powdered carbonate were extracted from PIM4 for $\delta^{18}O$ and $\delta^{13}C$ analyses using a computer-operated MicroMill Micro-Sampling Device with a 0.1 mm diameter drill bit. Sampling occurred along the central growth axis of the speleothem, with the first 20 mm from the top sampled with a 0.1 mm spacing, while from 20 mm to the bottom, a spacing of 0.2 mm was applied. For PIM5, 805 samples were obtained using a manual Sherline Mill with a 0.1 diameter drill bit, with a constant spacing of 0.4 mm along the central growth axis of the speleothem. All the carbonate powder samples were obtained at the Institute of Geoscience (University of São Paulo, Brazil).

For the construction of the age models the technique described in Campos et al. (2019) and Novello et al. (2021) was applied. Isotopic series were initially linearly interpolated between the ages to generate the geochronological models for the isotopic records. To merge the two $\delta^{18}O$ stalagmite records while accounting for the records' uncertainty, 1000 Monte-Carlo simulations were evaluated through the construction of age-depth models, accounting for the 1σ error in age using a Gaussian distribution random generator to simulate the age of chronological series, thereby generating 1000 age-depth models for each record. The isotopic time series were interpolated using the age models, resulting in 1000 proxies time-series. The two $\delta^{18}O$ records were merged through normalization (i.e., by subtracting the mean and dividing by the standard deviation) of the data inside the overlapping period, averaging both series and then reconstructing the shorter time series with the mean and standard deviation of the longer one, for each interpolated isotope time series (Monte-Carlo simulation).

3.2. Rainfall isotopic and cave monitoring

We discuss the modern climate data based on the rainfall captured at our monitoring station installed near the cave site (Pimenta Bueno city), where almost one full year of precipitation amount and rainwater $\delta^{18}O$ and δD data were collected (Sep. 2018–July 2019). Considering that data from only one annual hydrologic cycle at our rainfall monitoring station at the cave site was available, observational data from the Global Network of Isotopes in Precipitation (GNIP) of the two nearest meteorologic stations, Porto Velho (400 km distance) and Cuiabá (600 km distance), were used

to assist with the interpretation of the $\delta^{18}O_{precip}$ isotopic signature. Both these stations are influenced by the same climatic regime as our cave site.

For the cave monitoring, three watch glasses were placed inside the cave under three dripping points (PIM4, PIM6 and PIM8) in order to monitor oxygen and carbon isotopes of recent precipitated carbonate, and percolating water from the dripping points PIM6 and PIM8 points was collected for oxygen and deuterium isotope monitoring. In addition, two temperature-relative humidity data loggers (TH1 and TH2) were placed in distinct spots of the chamber over the course of one hydrological year (Sep. 2018–July 2019) to monitor the temperature and relative humidity of the cave atmosphere. TH1 was placed on the wall at a height close to the collected stalagmites and TH2 was located on top of the collapsed ceiling (~1.5 m below the current ceiling).

3.3. Model analysis

Data from the isotope-enabled Community Earth System Model (iCESM) (Brady et al., 2019) was used to interpret the dynamical controls on $\delta^{18}O$ at the location of the Cuíca record and to compare atmospheric dynamics during periods characterized by strong and weak E-W $\delta^{18}O$ gradients across the domain. iCESM is a fully-coupled state-of-the-art climate model with an approximate one degree horizontal grid spacing. The simulations evaluated were run with transient forcings from reconstructions covering the period 850–1850 CE, replicating those conducted for the non-isotope-enabled model Last Millennium experiments (Otto-Bliesner et al., 2016). Analysis of $\delta^{18}O$ of precipitation falling at Cuíca cave was based on rainy season (JFM) composites of three ensemble members forced by the full suite of external forcings to examine the circulation and hydroclimate dynamics associated with periods of enrichment and depletion of ^{18}O in precipitation. A precipitation-weighted $\delta^{18}O_{precip}$ ($\delta^{18}O$ from precipitation) time series was constructed for seasonal anomalies of each ensemble member. Due to the spatial uniformity of the $\delta^{18}O_{precip}$ signal and to smooth the internal variability of a single grid cell, the analyzed time series is derived from a 3×3 grid area average centered on the location of Cuíca cave. Composites were established based on seasonal anomalies of $\delta^{18}O_{precip}$ above and below a 2σ threshold relative to a given ensemble member mean, and the results were then averaged. Negative values in the composite are generally referred to in the text as “depleted” while positive anomalies are referred to as “enriched” in reference to more or less ^{18}O in the isotopic ratio. In addition to $\delta^{18}O_{precip}$, mid-tropospheric (524 hPa) vertical velocity (ω, negative values indicating upward motion) and precipitation fields were analyzed for the composited seasons. Composite plot stippling indicates grid cells where 90% of composited seasons agree on the sign of the anomaly (Fig. S4). A second analysis of the same parameters was performed to evaluate regional dynamics associated with periods of strong and weak gradients in $\delta^{18}O$ anomalies of precipitation between the Cuíca cave site and the Diva de Maura cave site (12°22′S, 41° 34′W) (Novello et al., 2012). For this analysis, composites are calculated for an extended austral summer season (JFMAM) to account for rainfall maxima at both sites. Composite plot stippling indicates grid cells where 90% of composited seasons agree on the sign of the anomaly. Statistical significance for all difference plots was tested for composites using a two-tailed student's t-test ($p < 0.05$) based on the total composite member differences.

3.4. Back-trajectory, clustering analysis and degree of rainout upstream (DRU)

Back-trajectories were computed for the monitoring period (September 2018 to July 2019) initiated at the location of the Cuíca cave (11°40′S, 60°38′W, ~310 m a.s.l.) using the HYbrid Single-Parcel Lagrangian Integrated Trajectory model 5 (Hysplit V5.1.0; Rolph et al., 2017; Stein et al., 2015). Daily back-trajectories were computed at 13 h, local time. The starting height was 1500 m a.s.l. (~850 hPa), as it represents the lower atmosphere, where the majority of moisture transport takes place. Considering that the global average water vapor residence time in the atmosphere is 8–10 days (Gimeno et al., 2021; Ent and Tuinenburg, 2017; Trenberth, 1998), air parcels were tracked back in time for 7 days, as this period covers potential fractionation processes along the moisture transport pathway (Ampuero et al., 2020; Hurley et al., 2012). The model was run with data from ERA 5 (Hersbach et al., 2020) with spatial resolution of $0.75° \times 0.75°$ and time step of 6 h starting at 0:00 UTC. Only back-trajectories with numerical error within tolerance and starting on precipitating days were selected. We consider a precipitating day when local precipitation is higher than 0.1 mm, computed with data from the Global Precipitation Measurement (GPM; Huffman et al., 2019) on a spatial resolution of $0.25° \times 0.25°$, as the average of 9 tiles centered at the Cuíca location. Thereby, we selected 236 back-trajectories. The cluster analysis of the final back-trajectories was computed with the clustering module of the Hysplit model, which applies a hierarchical clustering analysis (HCA) algorithm with Squared Euclidean distance. DRU was calculated with the wind back-trajectories, together with daily precipitation from GPM. We took GPM tiles along segments of 24 h length of each back-trajectory and two tiles width (0.5°). Then we integrated all the segments for each back-trajectory and summed up precipitation only in the continental grid cells. For comparison with the isotopic data, we used the weighted mean DRU values, based on local precipitation computed with GPM.

4. Results

4.1. Oxygen and carbon isotopic variability

The stalagmite PIM4 has an average 2σ U/Th age uncertainty of 0.025% or ±8 yrs and covers the period between 338 ± 5 to 2013 ± 3 yrs CE (Fig. 2), yielding a temporal resolution of 2.4 years for its isotopic profiles. Only a short 100-year hiatus was evident based on the geochronological model between 1046 ± 3 and 1146 ± 10 yrs CE. The segment used from PIM5 presents an average 2σ U/Th age uncertainty of 0.006% or ±13 yrs, spans from 1020 ± 12 yrs BCE to 587 ± 7 yrs CE (Fig. 2), resulting in an average 2-year resolution for the $\delta^{18}O$ and $\delta^{13}C$ records, and an overlap of about 200 years with PIM4. Since both samples share a similar range of $\delta^{18}O$ values during the overlapping period, combining the two samples provides a composite record of the last 3000 years from the southwestern Amazon basin, based on 37 U/Th ages with an average record resolution of 2 years.

The Cuíca cave $\delta^{18}O$ composite presents values ranging between −5.1 and −7.4‰ with a mean value of −6.6‰ (Fig. 3). From 1020 BCE until 0 ± 15 yrs CE the $\delta^{18}O$ values present a mean of −6.82‰, with a range of variability of ~0.6‰ and absence of a trend; between 0 and 850 ± 21 yrs CE the values increase until they reach a maximum value of −5.1‰ at about 850 CE. From 850 CE to 1800 ± 6 yrs CE a general trend towards more negative values prevails, yet two negative excursions occur, centered at 1260 CE (−6.7‰) and ~1740 ±3yrs CE (−7.1‰), which are separated by a positive excursion centered at 1370 CE (−5.5‰). From 1800 CE to the present, the $\delta^{18}O$ values remain stable, varying around the mean of −6.7‰, similar to the period before 850 CE.

The $\delta^{13}C$ record is characterized by a negative trend extending from its oldest portion until ~100 ± 11yrs CE, dropping from its highest value (−9.2‰) centered at ~980 ± 10yrs CE to its lowest

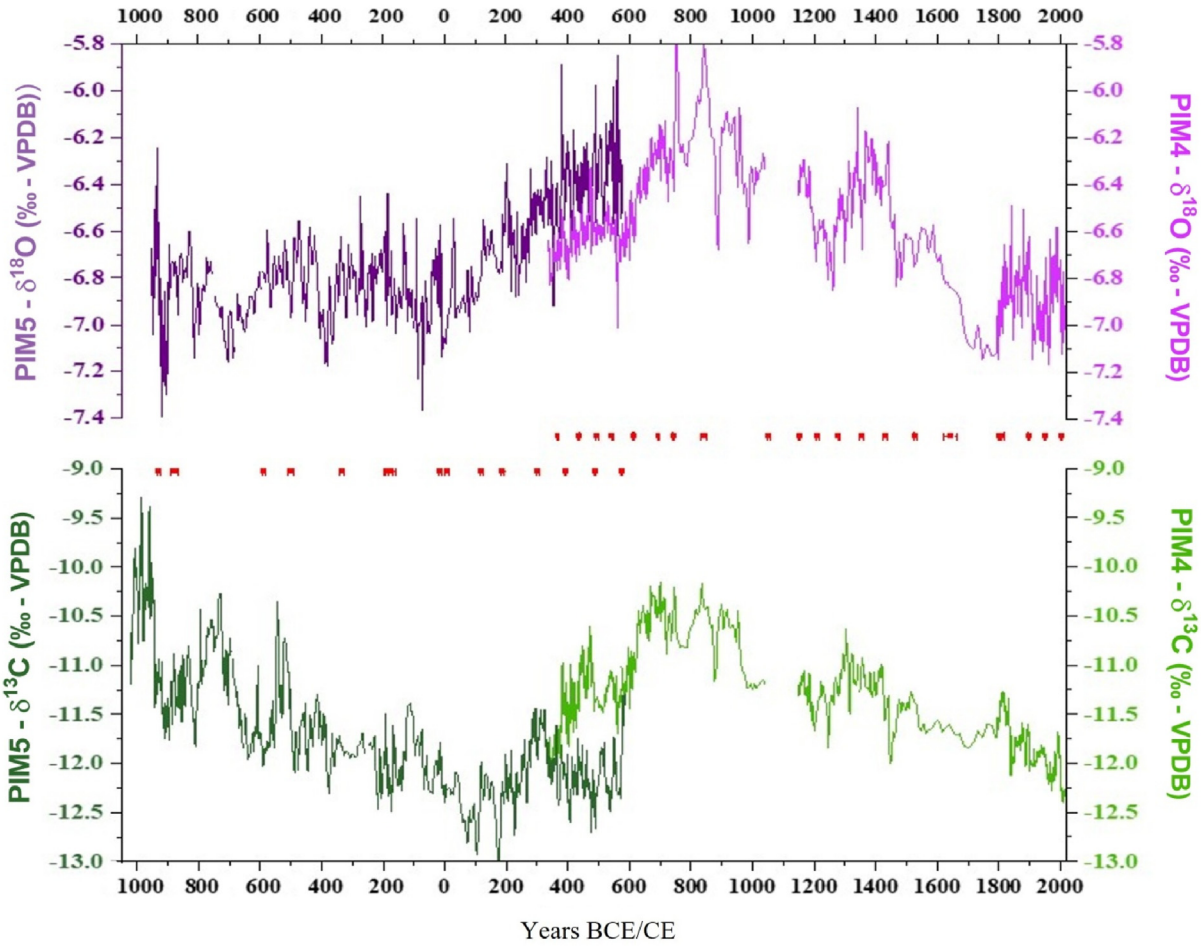

Fig. 2. (top) $\delta^{18}O$ stable isotope time series obtained from the stalagmites PIM4 (light purple) and PIM5 (dark purple). (bottom) $\delta^{13}C$ stable isotope time series obtained from the stalagmites PIM4 (light green) and PIM5 (dark green). U/Th ages and their corresponding error bars are shown in red between $\delta^{18}O$ and $\delta^{13}C$ records. The ages are represented in Common Era (CE, represented by the ages after the year 0) and Before Common Era (BCE, represented by the ages before year 0). (For interpretation of the references to color in this figure legend, the reader is referred to the Web version of this article.)

value centered at 170 ± 9 yrs CE, superimposed on centennial variability with an amplitude of 1.2‰, whereas the $\delta^{18}O$ is rather stable during this period (Figs. 2 and 6). From 170 CE until 1800 ± 6 yrs CE the $\delta^{13}C$ record displays trends which are consistent with those seen in the $\delta^{18}O$ record, but with reduced variability at decadal to centennial timescales. From 1800 CE onwards, the $\delta^{13}C$ trend differs from $\delta^{18}O$, continuing its decreasing trend until the present. The overlapping section of about 200 years (~400–600 CE) presents different $\delta^{13}C$ trends between PIM5 and PIM4, in contrast to what is being observed in the $\delta^{18}O$ record.

4.2. Isotope-enabled model analysis of climate influences

Composite analyses using the iCESM model with complete transient forcings over the last millennium document the regional hydroclimate associated with periods of strong depletion and enrichment in ^{18}O of the rainwater precipitating at Cuíca cave (Fig. S4. The composite analysis shows that precipitation depleted (enriched) in ^{18}O (Figs. S4g and h) corresponds to enhanced (reduced) upward motion over equatorial South America upstream of the cave site (Figs. S4a and b). The precipitation anomalies are largely co-located with regions of vertical motion anomalies, with rising motion triggering convective precipitation (Fig. S4d) and subsidence suppressing precipitation (Fig. S4e). Difference plots (Figs. S4c, f, i) highlight that while there is some correspondence between local changes in $\delta^{18}O_{precip}$ and co-located convection, the upstream activity dominates over the magnitude of local controls on isotopic extremes.

4.3. Wind back-trajectory analysis and DRU

Wind back-trajectory analysis for the monitoring period at Cuíca shows atmospheric transport pathways from the north-east (32%), east (33%), north-east local (12%), east local (12%) and south (2%) (Fig. S5). North-east and north local pathways are associated with the highest contribution to local annual precipitation and prevail during December–January -February (DJF). This season also presents the highest DRU values of the year and low $\delta^{18}O_{precip}$ of −8.19‰ on average (Fig. S6b). Although March–April – May (MAM) present lower local precipitation than DJF, the high DRU values may favor depletion of $\delta^{18}O_{precip,}$ with an average value of −9.33‰ (Fig. S6c). These results highlight the relevance of DRU relative to local precipitation at Cuíca.

5. Discussion

5.1. Results from cave monitoring and $\delta^{18}O$ interpretation in Amazonian stalagmites

The rain water $\delta^{18}O$ and δD collected weekly at the cave site,

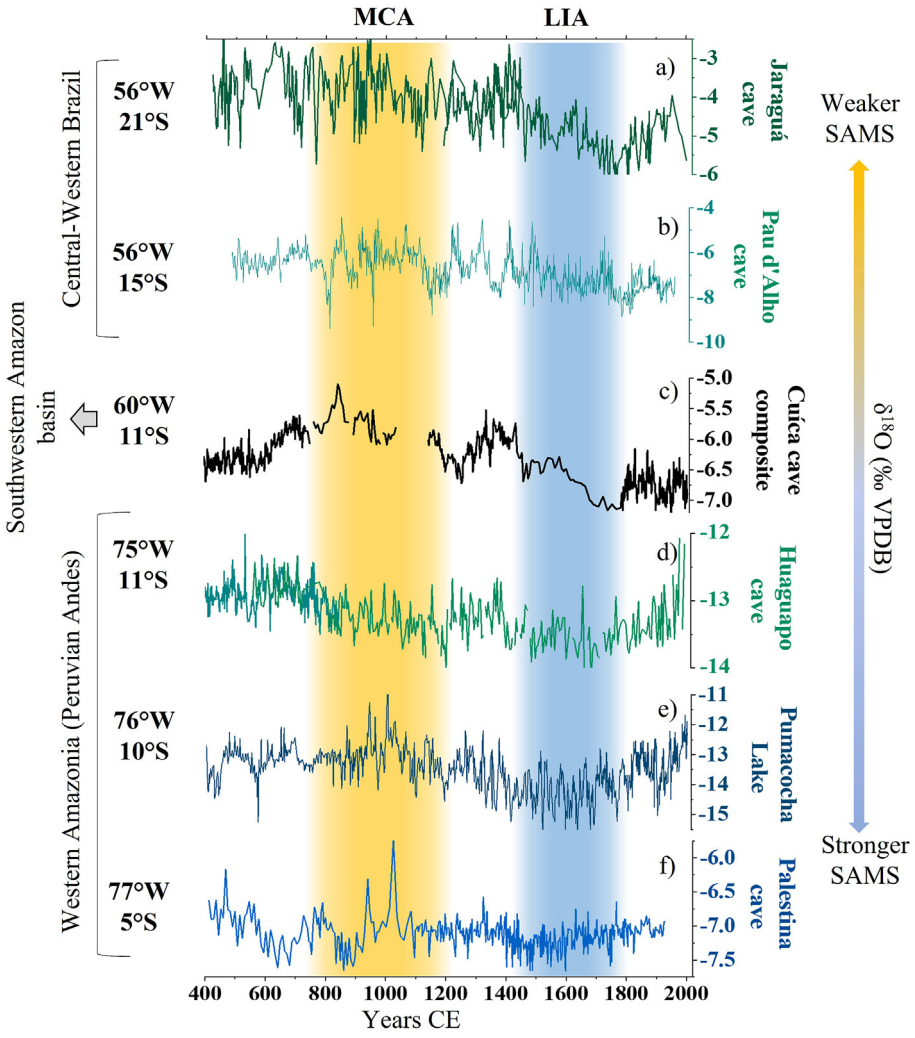

Fig. 3. - Comparison between the $\delta^{18}O$ records from western/southwestern Amazonia and Central-West Brazil. They are: a) Jaraguá cave (Novello et al., 2018) and b) Pau d'Alho cave (Novello et al., 2016) in central-western Brazil; c) Cuíca cave composite (this study) in the southwestern Amazon basin; d) Huagapo cave (Kanner et al., 2013), e) Pumacocha lake (Bird et al., 2011) and f) Palestina cave (Apaéstegui et al., 2014) in the western Amazon at the Andes foothills in Peru.

along with the isotopic data obtained from cave drip water collected during fieldwork, plot on top of the global meteoric water line (GMWL) (Fig. S7), demonstrating that the isotopic signal is not significantly affected by evaporation processes above the cave. Temperature recorded by TH1 in the room where the stalagmites were collected ranges between 24.2 and 25.9 °C, and TH2 recorded temperatures between 24.4 and 24.8 °C during this hydrologic year. Both devices registered 100% relative humidity during the monitored period (Fig. S8). These minor temperature variations recorded inside the cave throughout the year, and the relative humidity always being close to saturation avoid effects on the isotopic values from changes in the fractionation factor α and from evaporation. In addition, the fact that the $\delta^{18}O$ records of PIM5 and PIM4 covary during their overlapping period and the $\delta^{13}C$ record conversely decouples, provides further evidence for a climatic $\delta^{18}O$ signature rather than a kinetically driven signal, since $\delta^{18}O$ and $\delta^{13}C$ would strongly covary in the later scenario. Thus, the conditions in which the speleothems are formed in Cuíca cave are ideal for preserving the climatic signal embedded in the oxygen isotopes of the rainwater.

Regarding the processes that affect and control the $\delta^{18}O_{precip}$ isotopic signature, both amount effect and DRU (Ampuero et al., 2020) are considered here. While the amount effect reflects local precipitation, DRU integrates the upstream precipitation events, which better represents the physical mechanism of Rayleigh distillation for $\delta^{18}O_{precip}$ depletion. The $\delta^{18}O_{precip}$ observed at Cuíca is highly correlated with DRU ($r = -0.78$, $p < 0.01$) (Fig. S9 and Table S1), more so than with local precipitation ($r = -0.41$, $p < 0.01$). Although the rainfall amount is relevant for interpreting the $\delta^{18}O_{precip}$ composition at the Cuíca cave site, the results show that rainout along the path of easterly trade winds drives the isotopic depletion in water vapor that later condenses and rains out downstream (Ampuero et al., 2020; Vuille et al., 2012; Salati et al., 1979). This notion is corroborated by the regional dynamics observed in the iCESM model analyses (Fig. S3).

Hence, we interpret changes in the $\delta^{18}O$ record from Cuíca cave to be driven by the local rainfall isotopic composition, which is primarily affected by the DRU along the moisture trajectory from the Atlantic to the cave site. Since the DRU depends on the strength of monsoon-related convection upstream, we interpret the $\delta^{18}O$ speleothem record as a climate proxy for SAMS intensity in the region. Yet, given the location of Cuica cave close to the center of the monsoon core (e.g. see location with respect to the SASM index as defined by Vuille et al., 2012), precipitation at Cuica cave is a local

reflection of SAMS intensity, with the isotopic composition at this site incorporating both local and upstream processes. This interpretation is consistent with prior analyses of $\delta^{18}O$ records from speleothems and lakes located in the South American (sub-)tropics, and supported by a large number of studies relying on instrumental data, modelling, on-site calibration and multi-proxy comparisons (e.g. Bird et al., 2011; Vuille et al., 2012; Thompson et al., 2013; Novello et al., 2012, 2016, 2018, 2021; Apaéstegui et al., 2014; Moquet et al., 2016).

Our interpretation, however, differs from the analysis in Wang et al. (2017) based on speleothem records from the western Amazon basin during the last deglaciation. Wang et al. (2017) attributed the large $\delta^{18}O$ gradient during the last glacial period between Paraíso (eastern Amazon; ~ −4‰) and Tigre Perdido/Diamante (western Amazon; ~ −9‰) records to a decrease of rainforest coverage and density between the sites. The authors suggested that during the last glacial period the Amazon basin was drier, and the rainforest was diminished, which increased the $\delta^{18}O$ fractionation in the moisture that was transported from east to west due to reduced moisture recycling by the forest during its transit, while at times of higher vegetation density plant transpiration increased, thereby reducing the isotopic gradient between the sites. This interpretation, however, is not applicable to the late Holocene, as forest cover over the Amazon basin had long been established by 1000 BCE. Most sites where Amazon vegetation history has been reconstructed, show an increase in vegetation density starting in the mid-Holocene (after 6000 years BP) (Haberle and Maslin, 1999; Mayle and Power, 2008; Smith and Mayle, 2018; Kukla et al., 2021). Therefore, the significant differences observed in $\delta^{18}O$ between eastern and western Amazonian records during last millennia cannot be explained by changes in upstream plant transpiration and moisture recycling via forest changes (Fig. 4).

5.2. $\delta^{13}C$ data interpretation

$\delta^{13}C$ values measured in organic matter from soil profiles in Brazil, including near our study site, have been used to reconstruct vegetation dynamics during the Holocene period (Pessenda et al., 1998, 2001, 2009, 2010; Freitas et al., 2001; Gouveia et al., 2002). These studies show that soils under C_3 plants (mainly related to trees) present $\delta^{13}C$ values between −20‰ and −32‰, while C_4 plants (mainly related to grasses and to a more open vegetation) present $\delta^{13}C$ values between −9‰ and −17‰. $\delta^{13}C$ values in pedogenic carbonate are closely related to the isotopic values from the surrounding vegetation (Cerling, 1984; Quade, 1989), thus, Novello et al. (2021) using a collection of 25 stalagmites collated at different locations in tropical South America, such as Pau d'Alho and Curupira caves nearby Cuíca cave, show that the absolute $\delta^{13}C$

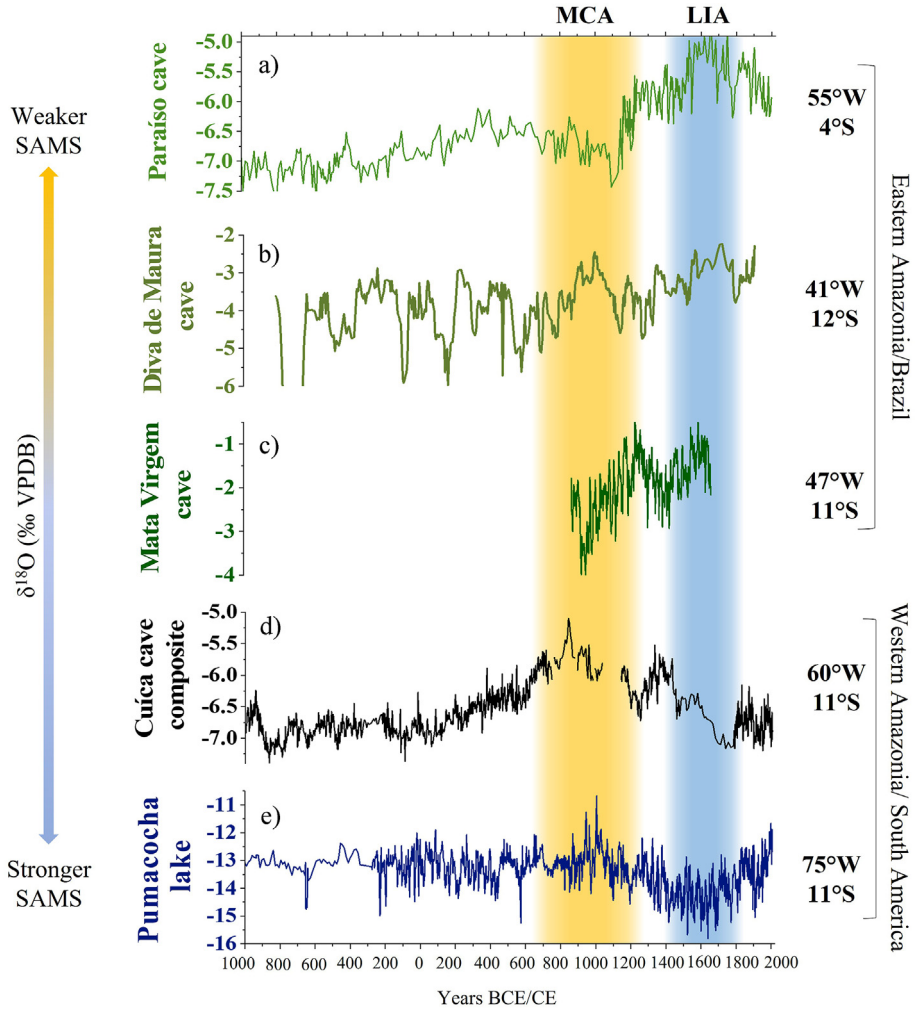

Fig. 4. - Comparison between the $\delta^{18}O$ records at opposite ends of the Amazon basin, displaying the east-west precipitation dipole. The sites are: a) Paraíso cave (Wang et al., 2017); b) Diva de Maura cave (Novello et al., 2012); c) Mata Virgem cave (Azevedo et al., 2019); d) Cuíca cave composite (this study); e) Pumacocha lake (Bird et al., 2011).

values in the stalagmites are indicative of the vegetation conditions above the cave. Furthermore, the authors attributed variations in $\delta^{13}C$ values in the stalagmites to prior calcite precipitation (PCP). PCP is forced by CO_2 degassing that preferentially removes ^{12}C from the solution to the cave atmosphere depleting ^{12}C in the final carbonate precipitated in the stalagmite (Baker et al., 1997; Mickler et al., 2019). PCP decreases during wetter periods due to the shorter exposure of the seepage solution to air that promotes significant calcite precipitation in the vadose zone while forming the stalagmites with lower $\delta^{13}C$ values in the cave galleries (Fairchild and Baker, 2012; Fohlmeister et al., 2020), and local wet conditions also increase biogenic CO_2 production by enhancing soil respiration rates, both contributing to more depleted $\delta^{13}C$ values in the stalagmites (Novello et al., 2021 and references therein). In addition, a longer wet period can favor C_3 (depleted in ^{13}C) over C_4 (enriched in ^{13}C) plants above the cave (Pessenda et al., 2010), providing a trend in the $\delta^{13}C$ values from the stalagmites (Novello et al., 2019). These mechanisms controlling $\delta^{13}C$ values in stalagmites (i.e. PCP, biogenic CO_2 production, and vegetation type above the cave) also contribute to a positive correlation between $\delta^{13}C$ and $\delta^{18}O$ in stalagmites located in regions where monsoons are the main provider of moisture and provide the main control on $\delta^{18}O$ variability (Mickler et al., 2006), hence monsoon intensity and local precipitation covary, as is the case in our study area (Novello et al., 2021).

Cuíca cave is located inside of the broad region studied by Novello et al. (2021), sharing the same characteristics as the other caves in western Amazonia/central-west Brazil. Furthermore, the Amazon region was not subjected to extensive changes in temperature through the last three millennia, avoiding significant temperature effects on the $\delta^{13}C$ values of the stalagmites (van Breukelen et al., 2008). Although it is not possible to quantify the contribution from each of these factors to the $\delta^{13}C$ values in our stalagmites, all factors mentioned above suggest that the $\delta^{13}C$ values from Cuíca cave may reflect local moisture conditions and soil/vegetation dynamics. To further investigate this, we compare and discuss our $\delta^{13}C$ stalagmite records with other paleoenvironmental records in section 5.4.

5.3. Paleoclimate dynamics over the Amazon Basin

The Cuíca $\delta^{18}O$ record documents the weakest SAMS activity between 700 and 1200 CE, and the strongest activity between 1400 and 1800 CE, reaching the weakest point around 850 CE. Overall, this is in accordance with other $\delta^{18}O$ records from western South America, such as Jaraguá cave (Novello et al., 2018) in southwestern Brazil (21°S/56°W), Pau D'Alho cave (Novello et al., 2016) in central-west Brazil (15°S/56°W), Huagapo cave (Kanner et al., 2013) and Pumacocha lake (Bird et al., 2011) in southern Peru (11°S/75°W), and Palestina cave (Apaéstegui et al., 2014) in northern Peru (5°S/77°W) (Fig. 3).

A weaker phase of the SAMS documented in the Cuíca record between 700 ± 4 and 1200 ± 8 yrs CE corresponds to the general drought during the Medieval Climate Anomaly (MCA) period documented in multiple $\delta^{18}O$ records from South America (Bird et al., 2011; Vuille et al., 2012; Novello et al., 2012, 2016, 2018; Apaéstegui et al., 2014). The pioneering high-resolution isotope records from South America first defined the MCA period in the continent between 900 and 1100 CE (Bird et al., 2011; Vuille et al., 2012), however, at Cuíca cave the corresponding dry period starts ~700 ±4yrs CE and is already well-established around 850–900 CE, lasting until 1200 CE. This early drier scenario before the MCA canonical period is also evident in the western Brazil records such as Jaraguá and Pau d'Alho caves, located to the west of the mean SACZ position. They display anomalously positive values at this time, likely indicating a decrease in moisture convergence over the SAMS/SACZ domain (Fig. 3). Enriched $\delta^{18}O$ values during the MCA are particularly evident in the Peruvian records of Pumacocha lake and Palestina and Huagapo caves, all located along the western margin of the SAMS domain. It is noteworthy, as previously mentioned, that the largest positive excursions of $\delta^{18}O$ in these western SAMS records that mark the MCA occur about 200 years later than at our site, which may reflect a stronger Pacific SST influence on climate at these higher elevation sites (Bird et al., 2011; Kanner et al., 2013; Apaéstegui et al., 2014). Thus, henceforth we will refer to this drier period in our record as MCA-phase. Following the MCA-phase, the time period between 1260 and 1450 CE is also marked by an anomalous drier period in the Cuíca record, although not as strong as during the MCA-phase. This anomaly is also observed in some of the other western Amazon records, such as Huagapo, Pumacocha and Jaraguá, all showing above-average $\delta^{18}O$ values during this period (Fig. 3).

In contrast, the following period (1450–1800 CE) corresponding to the Little Ice Age (LIA) (Vuille et al., 2012; Novello et al., 2018) is marked by enhanced SAMS activity at the Cuíca site. This is the time window during the last 3000 years where most of the paleoclimate records from western South America and central-west Brazil are synchronized (Fig. 3). At the beginning of the LIA period, the Cuíca $\delta^{18}O$ record drops by 1‰, resulting in values that are 2‰ more depleted than the highest values of the MCA-phase. Given that the Cuíca cave is located within the core region of SASM convective activity, this shift in the mean state towards a wetter LIA period indicates a strengthening of the monsoon over a large portion of the South American continent, affecting the isotopic composition of cave records from the northern Peruvian Andes to central-western Brazil (Fig. 3; Bird et al., 2011; Vuille et al., 2012; Kanner et al., 2013; Novello et al., 2016, 2018; Campos et al., 2019).

The drier-MCA-phase and wetter-LIA framework presented here is, however, not consistent for tropical South America as a whole, but only for the regions discussed this far (Novello et al., 2012; Wang et al., 2017; Campos et al., 2019; Azevedo et al., 2019). To illustrate the distinct climatic variability over tropical South America during these periods, we compare speleothem $\delta^{18}O$ records from the western Amazon (Pumacocha lake and Cuíca cave) with those from eastern Amazon/Brazil Nordeste (Paraíso and Mata Virgem cave, and Diva de Maura cave, respectively) (Fig. 4). The most distinct feature among all these records is the anti-phasing between wet conditions in the west (Pumacocha and Cuíca records) and the drier scenario over the eastern Amazon (Paraíso, Mata Virgem and Diva de Maura records) during the LIA period.

Even though the dipole feature over South America has been previously documented based on records in the Peruvian Andes and NEB (Thompson et al., 2013; Novello et al., 2018), here we introduce the Cuíca record to this discussion to assess this dynamic from the perspective of the core monsoon domain in the southwestern Amazon. In addition, we analyze the $\delta^{18}O$ gradient between the Cuíca and Diva de Maura caves, located over the western and eastern poles of the climate dipole, respectively (Fig. 5), in the CESM-iLME model. These results indicate that intensified upward motion and convection over the Cuíca cave region (southwestern Amazon) during periods with a strong $\delta^{18}O$ gradient is associated with enhanced subsidence over NEB and the Diva de Maura cave, resulting from an intensified upper-tropospheric wave guide, known as Bolivian High-Northeast Low system (Chen et al., 1999), and a contemporaneous southwesterly displacement of the SACZ (Novello et al., 2018). Hence, the enhanced $\delta^{18}O$ gradient between both sites reflects the surface expression of a dynamic, atmospherically-induced dipole pattern that can be observed in the isotopic proxy data during the LIA and is reproduced in the iCESM model at times when the simulated $\delta^{18}O$ values at the Cuíca cave

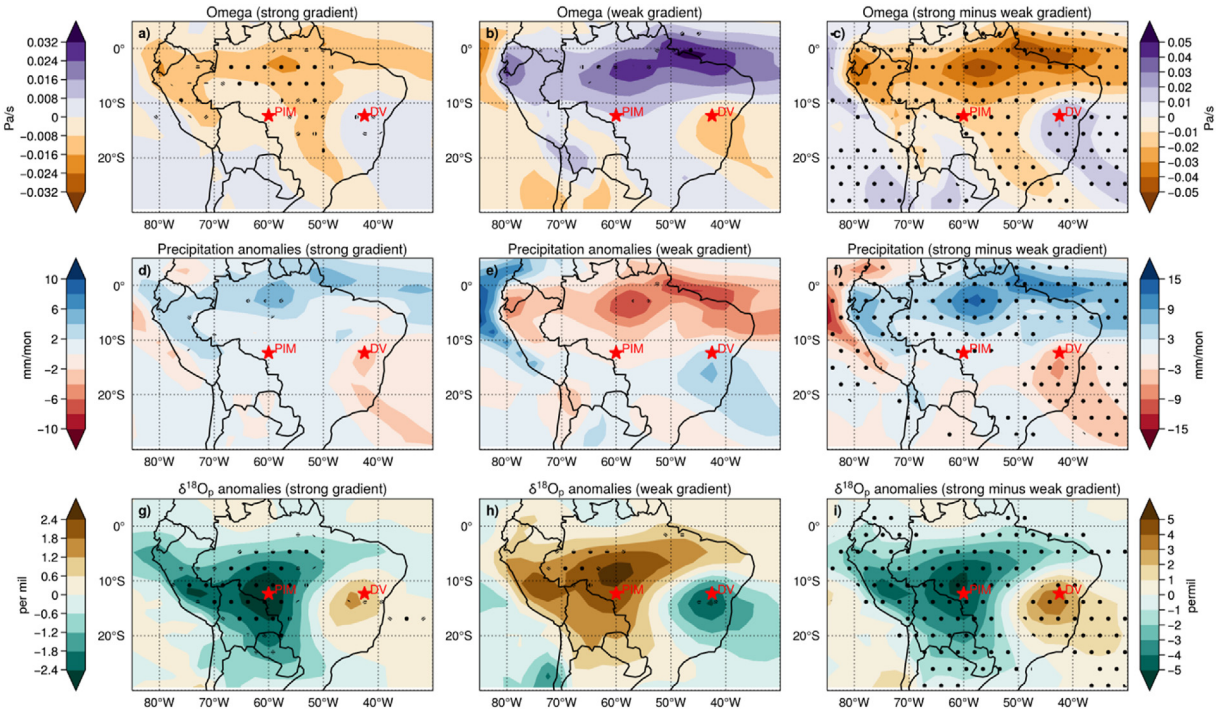

Fig. 5. Composite analysis of atmospheric dynamics and hydroclimate associated with the $\delta^{18}O$ gradient between Cuíca cave and Diva de Maura cave using the CESM-iLME full forcing experiment. The top row shows results for mid-tropospheric vertical motion (negative values indicating upward motion) at 524 hPa; middle row shows results for precipitation, and bottom row shows results for $\delta^{18}O_{precip}$. Cuíca cave and Diva de Maura cave locations are indicated with a red star in all plots. Composites are based on seasons below (column 1) and above (column 2) a 2σ threshold relative to the mean $\delta^{18}O_{precip}$ anomaly gradient between Cuíca cave and Diva de Maura cave, corresponding to anomalously strong and weak gradients, respectively. Column 3 shows the difference between an anomalously strong and weak gradient of $\delta^{18}O_{precip}$ anomalies. Stippling in the anomaly plots indicate grid cells where at least 90% of composited seasonal gradient anomalies share the same sign. Stippling in the difference plots show statistical significance between the two composites at $p < 0.05$. The left colorbar corresponds to columns 1, 2 and the right colorbar corresponds to column 3. (For interpretation of the references to color in this figure legend, the reader is referred to the Web version of this article.)

reach their most depleted values. Also, it is likely that the extended subsidence over NEB also affects the Mata Virgem region further to the west of Diva de Maura at 47°W, as well as the Paraíso region in the north-eastern Amazon at 55°W/4°S, in addition to a south-westward SACZ displacement (Novello et al., 2018). However, the largest changes seen in both mid-tropospheric vertical motion and precipitation are located upstream of the Cuíca site, suggesting that the local isotopic signal is reflective of larger-scale upstream circulation changes, rather than only local conditions, yet indicating an overall enhanced monsoon activity over the western side of the continent. Therefore, this striking anti-phased behavior during the LIA displays the clearest evidence for an east-west precipitation dipole over the Amazon region that is still present today (Chen et al., 1999; Sulca et al., 2016).

On the other hand, conditions were drier over both the core monsoon region (Cuíca and Pumacocha) and NEB (Diva de Maura) during the MCA-phase (Fig. 4), likely reflective of an overall reduction in moisture transport from the tropical Atlantic (Novello et al., 2012), whereas Paraíso and Mata Virgem records in the eastern Amazon present wetter conditions (Azevedo et al., 2019). The remarkable antiphasing between Cuica and Mata Virgem caves between 800 and 1600 CE suggests that the climate over the SW and SE Amazon basin was still antiphased and dynamically linked throughout the MCA-phase and transition into the LIA (Fig. 4c–d).

5.4. Paleoenvironmental changes in southwestern Amazonia and archeological implications

The decrease of the $\delta^{13}C$ values in the Cuíca record from 1000 BCE to 200 CE occurs without significant changes in the SAMS documented by the $\delta^{18}O$ record (Fig. 6). This is attributed to a progressive increase in vegetation density across the region, driven by a southward migration of the rainforest-savanna ecotone (Mayle et al., 2000; Burbridge et al., 2004). This southern expansion of rainforest vegetation is characterized by an increase in C_3 plant density over C_4 plants, which was also documented by the $\delta^{13}C$ measurements in several soil profiles separated by 200–500 km along a transect though Rondônia State (Pessenda et al., 1998, 2001; Freitas et al., 2001), and by the increase in Moraceae in Laguna Bella Vista (200 km south of Cuíca cave; Burbridge et al., 2004) during this period. In addition, an increase in Moraceae and decrease of Herbs in the pollen record from Laguna Chaplin (LCH) (Fig. 6) in northern Bolivia (14°S/61°W; Maezumi et al., 2018), 300 km south of Cuíca cave, also corroborates this interpretation. This is consistent with many paleovegetation reconstructions from the Amazon that documented a gradual southward expansion of humid tropical forest and a retraction of the seasonally dry tropical forest since the mid-Holocene (Haberle and Maslin, 1999; Mayle and Power, 2008; Taylor et al., 2010; Carson et al., 2014; Smith and Mayle, 2018).

The high $\delta^{13}C$ values in Cuíca during the MCA-phase may have been reinforced by the increase of the PCP due to low water availability at the cave epikarst given the general drier climate. Following the MCA-phase, a progressive trend toward more depleted Cuíca $\delta^{13}C$ values until the present indicates a vegetation expansion associated with more humid conditions. This is consistent with a vegetation change documented in the Laguna Bella Vista pollen record (Mayle et al., 2000; Burbridge et al., 2004; Maezumi et al., 2018) and in the soil profiles through Rondônia State (Pessenda et al., 1998, 2001; Freitas et al., 2001). Further south, the LCH record also documents an increase of % Moraceae and a

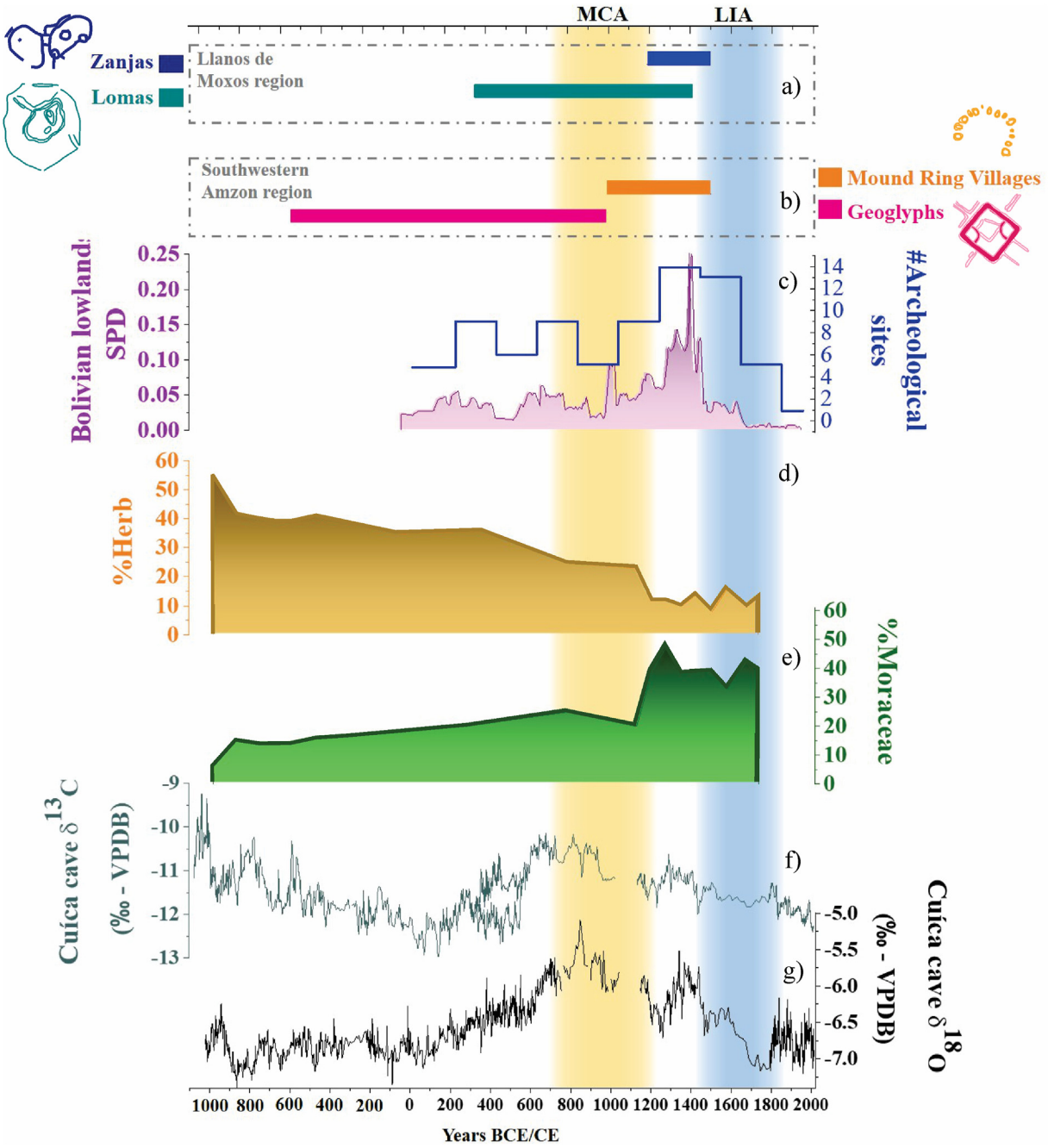

Fig. 6. a) Period of occurrence of archeological records from Llanos de Moxos region, comprising the Lomas (green) and Zanjas (blue) cultures (de Souza et al., 2019); b) same as in a), but from the southwestern Amazon region, comprising the Geoglyphs (pink) and Mound Ring Villages (orange) cultures (de Souza et al., 2019); c) SPD records from Bolivian lowland archeological sites and number of archeological sites within this region (Maezumi et al., 2018); Laguna Chaplin pollen records indicative of d) rainforest (%Moraceae) and of e) seasonally dry forest and savanna swamps (%Herbs) (Maezumi et al., 2018); Cuíca cave f) $\delta^{13}C$ and g) $\delta^{18}O$ records. (For interpretation of the references to color in this figure legend, the reader is referred to the Web version of this article.)

decrease in % Herbs, reflecting an ecotonal expansion of humid tropical forest that replaces seasonally dry forest and savanna swamps.

Recently, it has been proposed that pre-Columbian cultures were a major player responsible for vegetation changes during the last millennia in the Amazon Basin. Maezumi et al. (2018) compiled AMS-dates of the relationship between palaeofires and archeological sites from the Bolivian lowlands, which includes the location of Cuíca cave (Fig. 1), using the sum of the calibrated probability distribution (SPD) as an estimate of past population dynamics based on the density of ^{14}C ages in archeological sites. de Souza et al. (2019) further examined the relationship between speleothem records and the duration of archeological cultures in the *Llanos de Moxos* and the southwestern Amazon (namely, the state of Acre, Brazil) (Fig. 1). The former is characterized by two main archeological cultures – monumental mounds or *lomas* and ring ditches or *zanjas*. The latter is defined by the presence of geometrical enclosures (geoglyphs) and circular mound villages (de Souza et al., 2019) (Fig. 6). Although the studies performed by Maezumi et al. (2018) and de Souza et al. (2019) discussed several

paleoclimate records across the Amazon Basin, the climate conditions for Rondônia in their studies were extrapolated from paleoclimate records far away from the archeological sites. The new isotope data from Cuíca cave is strategically ideally located to contribute to a better understanding of these cultures, corroborating and complementing these previous archeological findings by filling an important gap in the isotopic paleo-network in the southwestern Amazon lowlands, not available at their time of publication.

Archeological evidence of human cultures exists near the Cuíca site for the period between ~600 BCE and 1500 CE (Fig. 6). The primary evidence comes from the geoglyphs, attributed to a culture that saw its demise prior to the European conquest during the drier conditions of the MCA-phase. On the other hand, new cultures (zanjas, lomas, mound ring villages) were established in the region around this time. Hence human populations flourished in the region during what was one of the driest periods according to our records, which was also marked by a retraction of the rainforest vegetation. The overall demise of the local population occurred in sync with the colonization of the continent after 1500 CE (Fig. 6). While it is difficult to associate the paleoecological and paleoclimatic conditions with human presence during the prehistorical period, the scenario presented here for the MCA-phase is similar to what was documented during the dry middle Holocene, where several studies, considering the evidence for earthworks (causeways, roads), suggested that human civilizations took advantage of a more open vegetation, to connect sites over long distances (Carson et al., 2014; Iriarte et al., 2020; Saunaluoma et al., 2021; Kukla et al., 2021).

6. Conclusions

The evidence presented here based on the new $\delta^{18}O$ record from Cuíca cave speleothems, supported by the isotope-enabled model analysis, indicates that the variations in $\delta^{18}O$ within the last 3000 years are indeed a reflection of monsoon variability and there is a notable dependence of $\delta^{18}O$ in precipitation on upstream rainout. Here we investigate the climatic variations throughout the Amazon basin over the last 3000 years characterized by four distinct periods: 1) 1020 BCE to 300 CE, when records throughout the basin point to a more uniform climatic pattern indicating neutral SAMS conditions; 2) The MCA-phase 700–1200 CE, with drier conditions established over the majority of the Amazon basin; 3) 1260–1450 CE, the transition period between the MCA and LIA periods characterized by heterogenous climate conditions over the Amazon basin; 4) 1450 to the present, marked by the establishment of an E-W precipitation dipole over the Amazon basin and, in a more expanded view, tropical South America, when the western-southwestern Amazon and central-western Brazil/SACZ regions are wetter compared to the drier eastern/northeastern regions.

The $\delta^{13}C$ record from Cuíca cave documents an expansion of rainforest vegetation between 1020 BCE and 200 CE, followed by a retraction and expansion during the MCA and LIA periods, respectively, indicating a general southward rainforest expansion during the late-Holocene as already proposed by paleovegetation studies performed on soil profiles in the region. The interplay between past climate and environmental changes with pre-Columbian cultures is complex and difficulties establishing cause-and-effect relationships abound. However, important demographic changes over the Amazon Basin seem to have occurred in association with important climatic and vegetation evolution documented in the Cuíca isotopic record.

Data availability

The new $\delta^{18}O$ and $\delta^{13}C$ records from Cuíca cave will be available at PANGAEA.

Author contributions

Marcela Eduarda Della Libera: Conceptualization, Validation, Formal analysis, Investigation, Writing of Original Draft, Writing of Review & Editing, Visualization. **Valdir Felipe Novello:** Supervision, Conceptualization, Validation, Writing of Original Draft, Writing – review & editing, Visualization. **Francisco William Cruz:** Supervision, Project administration, Funding acquisition, Conceptualization, Writing of Original Draft, Resources. **Rebecca Orrison:** Software, Formal analysis, Writing of Original Draft, Validation. **Mathias Vuille:** Supervision, Project administration, Funding acquisition, Conceptualization, Writing of Original Draft, Writing of Review & Editing, Validation. **Shira Yoshi Maezumi:** Writing of Original Draft. **Jonas de Souza:** Writing of Original Draft. **Julio Cauhy Rodrigues:** Investigation, Formal analysis, Writing of Original Draft, Visualization. **José Leandro Pereira Silveira Campos:** Software, Formal analysis. **Angela Ampuero:** Software, Formal analysis. **Giselle Utida:** Writing of Original Draft. **Nicolás Misailidis Stríkis:** Investigation. **Cintia Fernandes Stumpf:** Investigation. **Vitor Azevedo:** Investigation. **Haiwei Zhang:** Investigation. **R. Lawrence Edwards:** Resources. **Hai Cheng:** Resources.

Declaration of competing interest

The authors declare that they have no known competing financial interests or personal relationships that could have appeared to influence the work reported in this paper.

Acknowledgements

We thank the São Paulo Research Foundation (FAPESP) for financial support through grants 2018/25020-8 and 2019/22711-2 to M.E.D.L., 2016/15807-5 to VFN, 2017/50085-3 and 2019/07794-9 to FWC and the US National Science Foundation award OISE-1743738 to MV. We thank the Instituto Chico Mendes de Conservação da Biodiversidade (ICMBio) for providing the license (number 22424-8) to undertake the cave studies in Brazil.

Appendix A. Supplementary data

Supplementary data to this article can be found online at https://doi.org/10.1016/j.quascirev.2022.107383.

References

Ampuero, A., Stríkis, N.M., Apaéstegui, J., Vuille, M., Novello, V.F., Espinoza, J.C., Sifeddine, A., 2020. The forest effects on the isotopic composition of rainfall in the northwestern Amazon basin. J. Geophys. Res. Atmos. 125, 1–16. https://doi.org/10.1029/2019JD031445.

Apaéstegui, J., Cruz, F.W., Sifeddine, A., Espinoza, J.C., Guyot, J.L., Khodri, M., Santini, W., 2014. Hydroclimate variability of the northwestern Amazon basin near the Andean foothills of Peru related to the South American Monsoon System during the last 1600 years. Clim. Past 10, 1967–1981. https://doi.org/10.5194/cp-10-1967-2014.

Azevedo, V., Stríkis, N.M., Santos, R.A., Souza, J.G., Ampuero, A., Cruz, F.W., Edwards, R.L., 2019. Medieval Climate Variability in the eastern Amazon-Cerrado regions and its archeological implications. Sci. Rep. 9, 1–10. https://doi.org/10.1038/s41598-019-56852-7.

Baker, A., Ito, E., Smart, P., McEwan, R., 1997. Elevated and variable values of d13C. Chem. Geol. 136, 263–270. https://doi.org/10.1016/S0009-2541(96)00129-5.

Bird, B.W., Abbott, M.B., Vuille, M., Rodbell, D.T., Stansella, N.D., Rosenmeier, M.F., 2011. A 2,300-year-long annually resolved record of the South American summer monsoon from the Peruvian Andes. Proc. Natl. Acad. Sci. U. S. A 108 (21), 8583–8588. https://doi.org/10.1073/pnas.1003719108.

Brady, E., Stevenson, S., Bailey, D., Liu, Z., Noone, D., Zhu, J., 2019. The connected isotopic water cycle in the community Earth system model version 1. J. Adv. Model. Earth Syst. 11 (8), 2547–2566. https://doi.org/10.1029/2019MS001663.
Burbridge, R.E., Mayle, F.E., Killeen, T.J., 2004. Fifty-thousand-year vegetation and climate history of Noel Kempff Mercado National park, Bolivian Amazon. Quat. Res. 61, 215–230. https://doi.org/10.1016/j.yqres.2003.12.004.
Campos, J.L., Cruz, F.W., Ambrizzi, T., Deininger, M., Vuille, M., Novello, V.F., Strikis, N.M., 2019. Coherent south American monsoon variability during the last millennium revealed through high-resolution proxy records. Geophys. Res. Lett. 46 (14), 8261–8270. https://doi.org/10.1029/2019GL082513.
Carson, J.F., Whitney, B.S., Mayle, F.E., Iriarte, J., Prümers, H., Soto, J.D., Watling, J., 2014. Environmental impact of geometric earthworkconstruction in pre-Columbian Amazonia. Proc. Natl. Acad. Sci. Unit. States Am. 111 (29), 10497–10502. https://doi.org/10.1073/PNAS.1321770111.
Carvalho, L.M., Dias, M.A., 2020. Mesoscale and high-impact weather in the south American monsoon. In: Chih-Pei Chang, K.-J.H. (Ed.), The Multiscale Global Monsoon System. Naval Postgraduate School & National Taiwan University, p. 420.
Carvalho, L.M., Jones, C., Liebmann, B., 2002. Extreme precipitation events in southeastern south America and large-scale convective patterns in the south Atlantic convergence zone. J. Clim. 15, 2377–2394. https://doi.org/10.1175/1520-0442(2002)015<2377:EPEISS>2.0.CO;2.
Cerling, T., 1984. The stable isotopic composition of modern soil carbonate and its relationship to climate. Earth Planet Sci. Lett. 71 (2), 229–240. https://doi.org/10.1016/0012-821X(84)90089-X.
Chen, T.-C., Weng, S.-P., Schubert, S., 1999. Maintenance of austral summertime upper-tropospheric circulation over tropical South America: the Bolivian high–Nordeste low system. J. Atmos. Sci. 56 (13), 2081–2100. https://doi.org/10.1175/1520-0469(1999)056<2081:MOASUT>2.0.CO;2.
Cheng, H., Lawrence Edwards, R., Shen, C.C., Polyak, V.J., Asmerom, Y., Woodhead, J., Calvin Alexander, E., 2013a. Improvements in 230Th dating, 230Th and 234U half-life values, and U-Th isotopic measurements by multi-collector inductively coupled plasma mass spectrometry. Earth Planet Sci. Lett. 371–372, 82–90. https://doi.org/10.1016/j.epsl.2013.04.006.
Cheng, H., Sinha, A., Cruz, F.W., Wang, X., Edwards, R., d'Horta, F.M., Auler, A.S., 2013b. Climate change patterns in Amazonia and biodiversity. Nat. Commun. 4. https://doi.org/10.1038/ncomms2415.
Cruz, F., Vuille, M., Burns, S.J., Wang, X., Cheng, H., Werner, M., Nguyen, H., 2009. Orbitally driven east-west antiphasing of South American precipitation. Nat. Geosci. 2 (3). https://doi.org/10.1038/ngeo444.
de Souza, J.G., Robinson, M., Maezumi, S.Y., Capriles, J., Hoggarth, J.A., Lombardo, U., Iriarte, J., 2019. Climate change and cultural resilience in late pre-Columbian Amazonia. Nat. Ecol. Evol. 3, 1007–1017. https://doi.org/10.1038/s41559-019-0924-0.
Ent, R.J., Tuinenburg, O.A., 2017. The residence time of water in the atmosphere revisited. Hydrol. Earth Syst. Sci. 21, 779–790. https://doi.org/10.5194/hess-21-779-2017.
Fairchild, I.J., Baker, A., 2012. Speleothem Science: from Process to Past Environments. Wiley-Blackwell, West Sussex.
Fohlmeister, J., Voarintsoa, N.R., Lechleitner, F.A., Boyd, M., Brandtstatter, S., Jacobson, M.J., Oster, J.L., 2020. Main controls on the stable carbon isotope compositionof speleothems. Geochem. Cosmochim. Acta 279, 67–87. https://doi.org/10.1016/j.gca.2020.03.042.
Freitas, H., Pessenda, L., Aravena, R., Gouveia, S., RibeiroA, S., Boulet, R., 2001. Late Quaternary vegetation dynamics in the southern Amazon Basin inferred from carbon isotopes in soil organic matter. Quat. Res. 55 (1), 39–46. https://doi.org/10.1006/qres.2000.2192.
Gan, M.A., Kousky, V.E., Ropelewski, C.F., 2004. the South America monsoon circulation and its relationship to rainfall over west-Central Brazil. Am. Meteorol. Soc. 17, 47–66. https://doi.org/10.1175/1520-0442(2004)017<0047:TSAMCA>2.0.CO;2.
Gimeno, L., Eiras-Barca, J., Durán-Quesada, A.M., Dominguez, F., Ent, R.v., Sodemann, H., Kirchner, J.W., 2021. The residence time of water vapour in the atmosphere. Nat. Rev. Earth Environ. 2, 558–569. https://doi.org/10.1038/s43017-021-00181-9.
Gouveia, S., Pessenda, L., Aravena, R., Boulet, R., Scheel-Ybert, R., Bendassoli, J., Freitas, H., 2002. Carbonisotopes in charcoal and soils in studies of paleo-vegetation and climatechanges during the late Pleistocene and the Holocene in the southeast andcenterwest regions of Brazil. Global Planet. Change 33 (1–2), 95–106. https://doi.org/10.1016/S0921-8181(02)00064-4.
Haberle, S., Maslin, M., 1999. Late quaternary vegetation and climate change in the Amazon basin based on a 50,000 Year pollen record from the Amazon fan, ODP site 932. Quat. Res. 51 (1), 27–38. https://doi.org/10.1006/qres.1998.2020.
Hersbach, H., Bell, B., Berrisford, P., Hirahara, S., Horányi, A., Muñoz-Sabater, J., Thépaut, J.-N., 2020. The ERA5 global reanalysis. Q. J. R. Meteorol. Soc. 146 (730), 1999–2049. https://doi.org/10.1002/qj.3803.
Huffman, G., Stocker, E., Bolvin, D., Nelkin, E., Tan, J., 2019. GPM IMERG final precipitation L3 1 day 0.1 degree x 0.1 degree V06. In: Savtchenko, Andrey, Greenbelt, M.D. (Eds.), Goddard Earth Sciences Data and Information Services Center (GES DISC). https://doi.org/10.5067/GPM/IMERGDF/DAY/06.
Hurley, J.V., Galewsky, J., Worden, J., Noone, D., 2012. A test of the advection-condensation model for subtropical water vapor using stable isotopologue observations from Mauna Loa Observatory, Hawai. J. Geophys. Res. Atmos. 117, D19118. https://doi.org/10.1029/2011JD015773.
Iriarte, J., Elliot, S., Maezumi, S., Alves, D., Gonda, R., Robinson, M., Handley, J., 2020. The Origins of Amazonian Landscapes: Plant Cultivation, Domestication and the Spread of Food Production in Tropical South America, vol. 248, p. 106582. https://doi.org/10.1016/j.quascirev.2020.106582.
Kanner, L.C., Burns, S.J., Cheng, H., Edwards, R.L., Vuille, M., 2013. High-resolution variability of the South American summer monsoon over the last seven millennia: insights from a speleothem record from the central Peruvian Andes. Quat. Sci. Rev. 75, 1–10. https://doi.org/10.1016/j.quascirev.2013.05.008.
Kukla, T., Ahlströmb, A., Maezumi, S.Y., Chevaliere, M., Lu, Z., Winnick, M.J., Chamberlain, C.P., 2021. The resilience of Amazon tree cover to past and present drying. Global Planet. Change 202. https://doi.org/10.1016/j.gloplacha.2021.103520.
Liebmann, B., Kiladis, G.N., Vera, C.S., Saulo, A.C., Carvalho, L.M., 2004. Subseasonal variations of rainfall in south America in the vicinity of the low-level jet east of the Andes and comparison to those in the south Atlantic convergence zone. J. Clim. 17 (19), 3829–3842. https://doi.org/10.1175/1520-0442(2004)017<3829:SVORIS>2.0.CO;2.
Maezumi, S.Y., Whitney, B.S., Mayle, F.E., Souza, J.G., Iriarte, J., 2018. Reassessing climate and pre-Columbian drivers of paleofire activity in the Bolivian Amazon. Quat. Int. 488, 81–94. https://doi.org/10.1016/j.quaint.2017.11.053.
Marengo, J.A., Liebmann, B., Grimm, A.M., Misra, V., Dias, P.L., Cavalcanti, I.F., Alves, L.M., 2012. Recent developments on the South American monsoon system. Int. J. Climatol. 32, 1–21. https://doi.org/10.1002/joc.2254.
Mayle, F.E., Power, M.J., 2008. Impact of a drier early–mid-holocene climate upon Amazonian forests. Philos. Trans. Royal Soc. B 363 (1498), 1829–1838. https://doi.org/10.1098/rstb.2007.0019.
Mayle, F.E., Burbridge, R., Killeen, T.J., 2000. Millennial-scale dynamics of southern Amazonian rain forests. Science 290, 2291–2294. https://doi.org/10.1126/science.290.5500.2291.
Mickler, P., Carlson, P., Banner, J., Breecker, D., Stern, L., Guilfoyle, A., 2019. Quantifying Carbon Isotope Disequilibrium during In-Cave Evolution of Drip, vol. 244, pp. 182–196. https://doi.org/10.1016/j.gca.2018.09.027.
Mickler, P., Stern, L., Banner, J., 2006. Large Kinect isotope effects in modern speleothems. Geol. Soc. Am. Bull. 118, 65–81. https://doi.org/10.1130/B25698.1.
Miranda, I.S., 2000. Floristic and structural analysis of wood vegetation of comemoração river, Pimenta Bueno, Rondônia, Brazil. Acta Amazonica 30 (3). https://doi.org/10.1590/1809-43922000303422.
Moquet, J.-S., Guyot, J.-L., Crave, A., Viers, J., Filizola, N., Martinez, J.-M., Pombosa, R., 2016. Amazon River dissolved load: temporal dynamics and annual budget from the Andes to the ocean. Environ. Sci. Pollut. Control Ser. 23, 11405–11429. https://doi.org/10.1007/s11356-015-5503-6.
Novello, V.F., Cruz, F.W., Karmann, I., Burns, S.J., Stríkis, N.M., Vuille, M., Barreto, E.A., 2012. Multidecadal climate variability in Brazil's Nordeste during the last 3000 years based on speleothem isotope records. Geophys. Res. Lett. 39 (23), 1–6. https://doi.org/10.1029/2012GL053936.
Novello, V.F., Cruz, F.W., Moquet, J.S., Vuille, M., Paula, M.S., Nunes, D., Campos, J.L., 2018. Two millennia of South Atlantic convergence zone variability reconstructed from isotopic proxies. Geophys. Res. Lett. 45 (10), 5045–5051. https://doi.org/10.1029/2017GL076838.
Novello, V.F., Vuille, M., Cruz, F.W., Stríkis, N.M., De Paula, M.S., Edwards, R.L., Moquet, J.S., 2016. Centennial-scale solar forcing of the South American Monsoon System recorded in stalagmites. Sci. Rep. 6, 1–8. https://doi.org/10.1038/srep24762.
Novello, V.F., William da Cruz, F., Vuille, M., Pereira Silveira Campos, J.L., Stríkis, N.M., Apaéstegui, J., Karmann, I., 2021. Investigating δ13C values in stalagmites from tropical South America for the last two millennia. Quat. Sci. Rev. 255, 1–10. https://doi.org/10.1016/j.quascirev.2021.106822.
Otto-Bliesner, B.L., Brady, E.C., Fasullo, J., Jahn, A., Landrum, L., Stevenson, S., Strand, G., 2016. Climate variability and change since 850 CE: an ensemble approach with the community Earth system model. Bull. Am. Meteorol. Soc. 97 (5), 735–754. https://doi.org/10.1175/BAMS-D-14-00233.1.
Pessenda, L., Boulet, R., Aravena, R., Rosolen, V., Gouveia, S., Ribeiro, A., Lamotte, M., 2001. Origin and dynamics of soil organic matter and vegetation changes during the Holocene in a forest-savanna transition zone, Brazilian Amazon Region. Holocene 11 (2), 250–254. https://doi.org/10.1191/095968301668898509.
Pessenda, L., De Oliveira, P., Mofatto, M., Medeiros, V., Garcia, R., Aravena, R., Etchebehere, M., 2009. The evolution of a tropical rainforest/grassland mosaic in southeastern Brazil since 28,000 14C yr BP based on carbon isotopes and pollen records. Quat. Res. 71 (3), 437–459. https://doi.org/10.1016/j.yqres.2009.01.008.
Pessenda, L., Gomes, B., Aravena, R., Ribeiro, A., Boulet, R., Gouveia, S., 1998. The carbon isotope record in soils along a forest-cerrado ecosystem transect: implications for vegetation changes in the Rondônia State, southwestern Brazilian Amazon region. Holocene 8 (5), 599–603. https://doi.org/10.1191/095968398673187182.
Pessenda, L., Gouveia, S., Ribeiro, A., Oliveira, P., Aravena, R., 2010. Late Pleistocene and Holocene vegetation changes in northeastern Brazil determined from carbon isotopes and charcoal records in soil. Palaeogeogr. Palaeoclimatol. Palaeoecol. 297, 597–608. https://doi.org/10.1016/j.palaeo.2010.09.008.
Quade, J.C., 1989. 9. Systematic variations in the carbon andoxygen isotopic composition of pedogenic carbonate along transects in theSouthern Great Basin, United States. Geol. Soc. Am. Bull. 101, 464–475. https://doi.org/10.1130/0016-7606(1989)101<0464:SVITCA>2.3.CO;2.
Raia, A., Cavalcanti, I.F.A., 2008. The life cycle of the South American monsoon system. J. Clim. 21 (23), 6227–6246. https://doi.org/10.1175/2008JCLI2249.1.
Rolph, G., Stein, A., Stunder, B., 2017. Real-time Environmental Applications and

Display sYstem: READY, vol. 95. Environmental Modelling & Software, pp. 210–228. https://doi.org/10.1016/j.envsoft.2017.06.025.
Salati, E., Dall'Olio, A., Matsu, E., Gat, J.R., 1979. Recycling of water in the Amazon basin: an isotopic study. Water Resour. Res. 15 (5), 1250–1258 doi:0043-1397/79/009 W-0552501.00.
Saunaluoma, S., Moat, J., Pugliese, F., Neves, E., 2021. Patterned villagescapes and road networks in ancient southwestern Amazonia. Lat. Am. Antiq. 32, 173–187. https://doi.org/10.1017/laq.2020.79.
Smith, R.J., Mayle, F.E., 2018. Impact of mid- to late Holocene precipitation changes on vegetation across lowland tropical South America: a paleo-data synthesis. Quat. Res. 89 (1), 134–155. https://doi.org/10.1017/qua.2017.89.
Stein, A., Draxler, R., Rolph, G., Stunder, B., Cohen, M., Ngan, F., 2015. NOAA's HYSPLIT atmospheric transport and dispersion modeling system. Bull. Am. Meteorol. Soc. 96 (12), 2059–2077. https://doi.org/10.1175/BAMS-D-14-00110.1.
Sulca, J., Vuille, M., Silva, Y., Takahashi, K., 2016. Teleconnections between the Peruvian central Andes and northeast Brazil during extreme rainfall events in austral summer. J. Hydrometeorol. 17 (2), 499–515. https://doi.org/10.1175/JHM-D-15-0034.1.
Taylor, Z.P., Horn, S.P., Mora, C.I., Orvis, K.H., Cooper, L.W., 2010. A multi-proxy paloecological record of late-Holocene forest expansion in lowland Bolivia. Paleogeogr. Paleoclimatol. Paleoecol. 293, 98–107. https://doi.org/10.1016/j.paleo.2010.05.004.
Thompson, L.G., Mosley-Thompson, E., Davis, M.E., Zagorodnov, V.S., Howat, I.M., Mikhalenko, V.N., Lin, P.-N., 2013. Annually resolved Ice core records of tropical climate variability over the past ~1800 years. Science 340 (6135), 945–950. https://doi.org/10.1126/science.1234210.
Trenberth, K.E., 1998. Atmospheric moisture residence times and cycling: implications for rainfall rates and climate change. Climatic Change 39, 667–694. https://doi.org/10.1023/A:1005319109110.
van Breukelen, M., Vonhof, H., Hellstrom, J., Wester, W., Kroon, D., 2008. Fossil dripwater in stalagmites reveals Holocene temperature and rainfall variation in Amazonia. Earth Planet Sci. Lett. 275 (1–2), 54–60. https://doi.org/10.1016/j.epsl.2008.07.060.
Vera, C., Baez, J., Douglas, M., Emmanuel, C.B., Marengo, J., Meitin, J., Zipser, E., 2006. The South American low-level jet experiment. Bull. Am. Meteorol. Soc. 87 (1), 63–77. https://doi.org/10.1175/BAMS-87-1-63.
Vuille, M., Burns, S.J., Taylor, B.L., Cruz, F.W., Bird, B.W., Abbott, M.B., Novello, V.F., 2012. A review of the South American monsoon history as recorded in stable isotopic proxies over the past two millennia. Clim. Past 8 (4), 1309–1321. https://doi.org/10.5194/cp-8-1309-2012.
Wang, X., Edwards, R.L., Auler, A.S., Cheng, H., Kong, X., Wang, y., Chiang, H.-W., 2017. Hydroclimate changes across the Amazon lowlands over the past 45,000 years. Nature 541 (7636), 204–207. https://doi.org/10.1038/nature20787.
Werth, D., Avissar, R., 2002. The local and global effects of Amazon deforestation David. J. Geophys. Res. 107, 55.1–55.8.
Zilli, M.T., Carvalho, L.M., Lintner, B.R., 2019. The poleward shift of South Atlantic Convergence Zone in recent decades. Clim. Dynam. 52 (5–6), 2545–2563. https://doi.org/10.1007/s00382-018-4277-1.